Deformation of Rubber-Toughened Polycarbonate: Microscale and Nanoscale Analysis of the Damage Zone

C. CHENG,[1,*] A. HILTNER,[2,†] E. BAER,[1] P. R. SOSKEY,[2] and S. G. MYLONAKIS[2]

[1]Department of Macromolecular Science, and Center for Applied Polymer Research, Case Western Reserve University, Cleveland, Ohio 44106; [2]EniChem America Inc., Research and Development Center, 2000 Cornwall Rd., Monmouth Junction, New Jersey 08852

SYNOPSIS

Deformation of polycarbonate (PC) impact-modified with a core–shell rubber (MBS) was examined at the microscale and nanoscale. The stress-whitened zone (SWZ) that formed ahead of a semicircular notch was sectioned and examined in an optical microscope and transmission electron microscope. At the microscale, the texture of the SWZ consisted of fine shear lines that formed when cavitation of the rubber particles relieved triaxiality and enabled the PC matrix in the SWZ to deform in shear. Examination of thin sections from the SWZ in the transmission electron microscope revealed nanoscale deformation of the rubber particles. When the particle concentration was low (2%), only random cavitation of rubber particles was observed. At higher particle concentrations (5 and 10%), cooperative cavitation produced linear arrays of cavitated particles. The matrix ligaments between cavitated particles were strong enough that they did not fracture; higher strains were accommodated by particle cavitation and matrix extension in the regions separating the arrays. The cavitated arrays were also observed in the damage zone that accompanied the fracture surface of specimens impacted at −20°C. Cooperative cavitation may have implications for the impact strength of blends with higher concentrations of rubber particles. The possibility that particle–particle interactions facilitate cavitation and promote matrix shear deformation is especially relevant to low-temperature impact strength. © 1995 John Wiley & Sons, Inc.

INTRODUCTION

The notch sensitivity of ductile thermoplastics such as polycarbonate (PC), nylon, and poly(vinyl chloride) is attributed to the formation of a critical-size internal craze. Ahead of a semicircular notch, the internal craze initiates at the plastic–elastic boundary where the triaxial stresses are highest.[1] The presence of dispersed rubber particles in the matrix provides an alternative cavitation mechanism that relieves the triaxiality before an internal craze can initiate. Once the rubber particles cavitate, the ductile matrix deforms in shear. It is generally thought that the primary energy absorption mechanism in toughened PC is shear deformation of the matrix, rather than cavitation of the rubber particles. Nevertheless, the properties of the rubber are important. There is evidence that rubber particles with higher cavitation resistance impart better toughness to PC.[2] The rubber can also strengthen the PC ligaments between cavitated particles and prevent coalescence into critical size voids.[3]

The semicircular notch is attractive for studies of prefracture deformation when the goal is to examine the deformation in a triaxial stress state while minimizing the tendency for crack growth. We used this geometry to determine the cavitation condition of some core–shell rubbers in PC.[2] A critical mean stress and the corresponding volume strain were obtained by a macromechanics analysis of the stress-whitened zone. Because there was no particle concentration dependence, these parameters appear to

* Present address: 3M Company, St. Paul, MN 55144.
† To whom correspondence should be addressed.

Journal of Applied Polymer Science, Vol. 55, 1691–1702 (1995)
 CCC 0021-8995/95/121691-12

describe the initiation condition for random cavitation of single particles. This analysis does not address subsequent events that may include, in addition to shear deformation of the matrix, further particle cavitation and possibly coalescence of cavitated rubber particles. Cooperative cavitation in rubber-modified PC becomes more likely as the interparticle separation decreases. One macroscale observation that depends on particle concentration is the shape of the stress-whitened zone. This may be a manifestation of interactive microdeformation mechanisms. To identify interactive cavitational phenomena in rubber-modified PC, studies of particle deformation at the microscale and nanoscale are required. This article describes our optical and electron microscopic studies of deformation processes in rubber-modified PC and the hierarchical models that represent these observations.

MATERIALS AND METHODS

The matrix polymer was a commercial polycarbonate (PC), produced by EniChem SpA, designated as Sinvet 251, with a molecular weight of about 32,000. The MBS impact modifier was Paraloid EXL-3607 (PL) from Rohm and Haas Co. The monodisperse PL particles were 0.2 μm in diameter.

The starting materials were extruded as described previously[2] and injection-molded into ASTM D638 dogbone-shaped specimens 3.14 mm in thickness. A 1 mm-radius semicircular notch was machined with an end mill midway along one edge of the tensile specimens. The notched specimens were mounted in an Instron machine with 115 mm separating the grips and loaded at a crosshead speed of 0.1 mm/min at ambient temperature unless otherwise specified.

A 300 μm-thick section was cut from the midplane of the damage zone with an Isomet diamond saw and then further polished to a thickness of 40–70 μm with petrographic polishing techniques. The polished sections were viewed in the optical microscope in the transmission mode.

Sections for transmission electron microscopy (TEM) were prepared by embedding a 300 μm-thick section in epoxy resin, Hysol RE-2038 from Dexter, which cured in 8 h at ambient temperature. The block was carefully trimmed with a glass knife, with the assistance of an optical microscope operated in the reflection mode, to expose the desired region of the damage zone. The block was then stained by immersion for 3 days in a 2% aqueous solution of osmium tetroxide, and thin sections were wet cryomicrotomed with a diamond blade in an RMC MT6000-XL ultramicrotome equipped with a CR-2000 cryosectioning unit. The specimen temperature was −90°C and the knife temperature was −50°C. The 90–120 nm sections were examined in a JEOL 100SX transmission electron microscope.

Particle size and cavity size were analyzed with an Olympus Cue-4 image analysis system. The micrographs were scanned by a high-resolution charge-coupled device camera (500 × 582 pixels), and the image was transmitted to the image monitor and analyzed on a personal computer. The sizes of 150 or more particles or cavities were measured and the average value was reported.

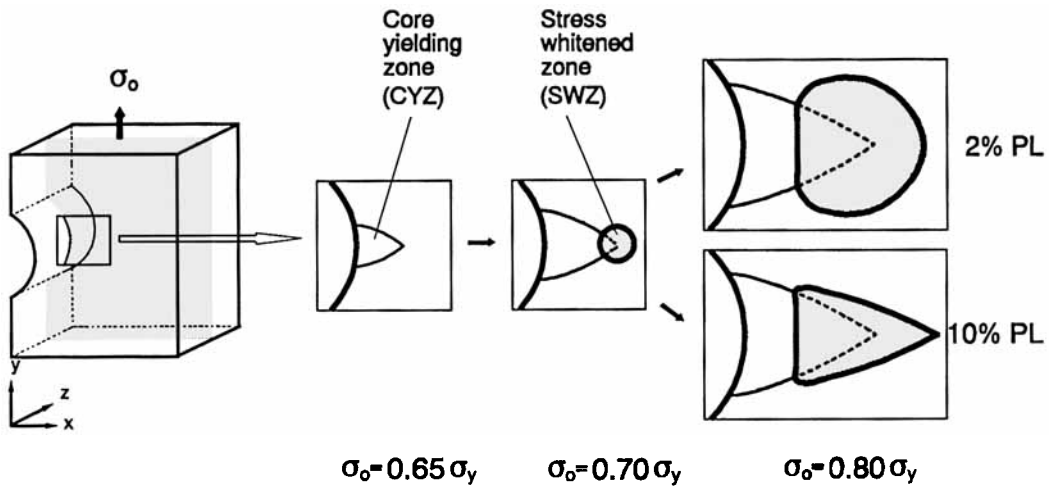

Figure 1 Schematic illustration of the macroscopic deformation zone in blends of PC with PL rubber as it grows ahead of a semicircular notch during tensile loading.

RESULTS AND DISCUSSION

Macroscale and Microscale Deformation

The sketch in Figure 1 of the macroscopic appearance of the deformation zone in blends of PC with PL rubber as it grows ahead of a semicircular notch during tensile loading is based on results published previously.[2] Yielding in the center of the specimen at the notch root begins when the remote stress reaches about 60% of the tensile yield stress (0.6 σ_T). The yielded region, designated as the core yielding zone (CYZ), consists of two sets of slip lines that grow out from the notch root. The slip lines in the blends are thinner and more numerous than those in unmodified PC, which is consistent with delocalization of matrix shear yielding by the rubber particles. At a slightly higher stress, a dark region appears at the tip of the CYZ. The darkness is caused by light scattering from cavitated rubber particles, and, therefore, this region is designated as the stress-whitened zone (SWZ). From the position of the SWZ relative to the notch root, the critical condition for cavitation can be determined.[2] The SWZ is circular in shape when it first appears; if the rubber content is fairly low, about 2%, the zone retains the circular shape as it increases in size with increasing stress. With higher rubber content, 5 and 10%, the shape gradually changes from circular to triangular.

The change in overall shape of the SWZ as the rubber content increased from 2 to 5 to 10% is clearly shown in the optical micrographs in Figure 2. These micrographs were obtained after the specimens were loaded to 0.8 σ_T, sectioned through the center of the thickness (xy plane), and polished. The near notch boundary of the SWZ is located 0.30–0.35 mm from the notch root, and the far notch boundary, about 1.0 mm from the notch root. The CYZ is not visible in these micrographs; it was only visible in the optical microscope when the specimen was examined under crossed polars. The optical micrographs also show a texture in the SWZ of fine dark lines oriented in the shear directions. The shear lines intersected at an angle of 60°–65° in the x-direction (normal to the loading direction); it decreased slightly with increasing rubber content from 65° to 61° to 59° for 2, 5, and 10% rubber, respectively. The shear lines became coarser as the rubber content increased. The intersection angle was somewhat less than the 85° for pressure-dependent yielding of PC.[2] It has been pointed out that preexisting voids have the effect of increasing the pressure sensitivity of the yield criterion.[4] Consequently, the shear lines rotate away from the major principal stress axis. The model accounts for both the magnitude of the effect and the dependence on particle content found in the SWZ.

For convenience, the SWZ ahead of a semicircular notch of radius a was divided into two regions: The near notch region extended from the near notch boundary at 0.3 a to the tip of the CYZ, which for a remote stress of 0.8 σ_T was calculated from slip line theory to be a distance 0.6 a from the notch root. The far notch region extended from the tip of the CYZ to the far notch boundary of the SWZ. The intersection angle of the shear lines in the near notch region of the SWZ was in the range of 60°–65°. Fur-

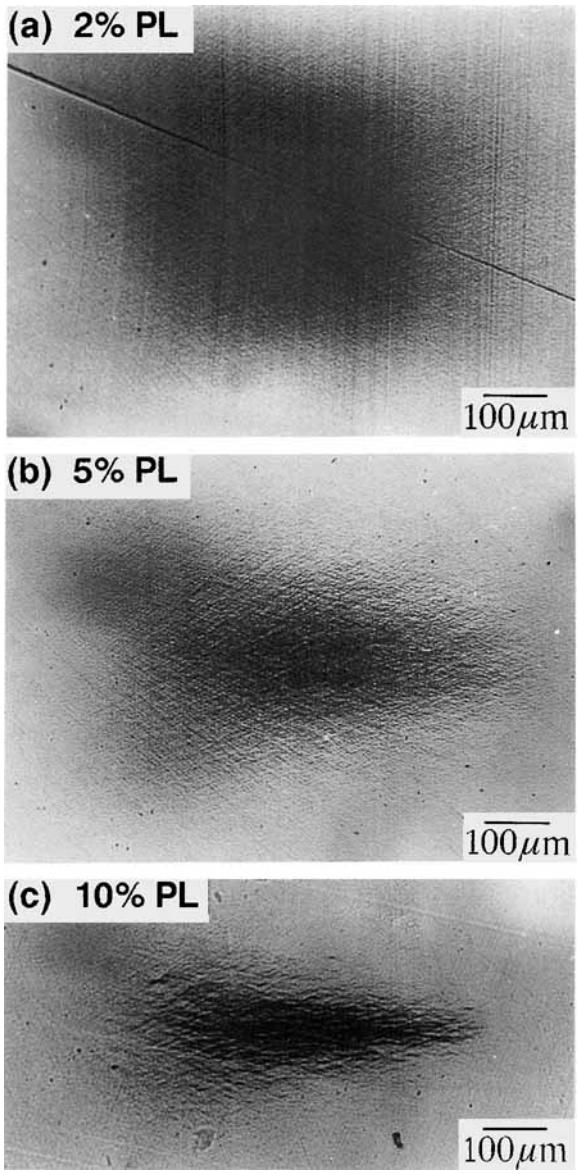

Figure 2 Optical micrographs of the SWZ in the xy plane at 0.8 σ_T: (a) 2% PL; (b) 5% PL; (c) 10% PL. Specimens were polished to a thickness less than 0.1 mm.

ther from the notch, the angle depended strongly on the rubber content: It remained at about 65° throughout the SWZ of the 2% PL, but gradually decreased away from the notch root in the blends with 5 and 10% rubber. In the far notch region, the shear lines intersected at an angle of about 48° in the blend with 5% PL. The texture in the far notch region of the blend with 10% PL consisted of irregular, wavy lines oriented almost parallel to the x-direction.

The near notch region of the SWZ in the blend with 10% PL was sectioned through the other two orthogonal planes. In cross section (yz plane), the SWZ had an oblong shape that did not extend to the surfaces. Confinement of stress-whitening to the center of the specimen reflected the requirement for a triaxial stress state. The texture of the SWZ in the yz plane was the same as in the xy plane and consisted of dark shear lines that intersected at an angle of about 60° [Fig. 3(a)]. The shear lines were not visible in the plane normal to loading (xz plane); instead, the texture of the stress-whitening consisted of uniformly distributed 1–3 μm dark spots [Fig. 3(b)].

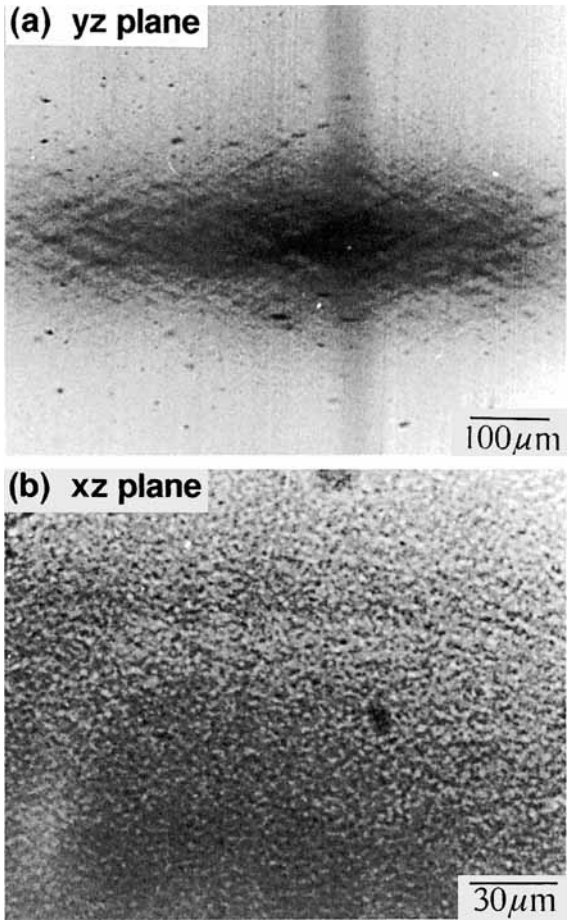

Figure 3 Optical micrographs of the SWZ in PC with 10% PL at 0.8 σ_T: (a) yz plane; (b) xz plane. Specimens were polished to a thickness less than 0.1 mm.

The shear texture seen in the blends is not observed ahead of a circular or semicircular notch in unmodified PC. Shear deformation in PC is confined to slip lines of the CYZ until macroscopic, through thickness flow leads to global yielding.[5] Under the triaxial stress state ahead of a semicircular notch, cavitation of rubber particles in the blend relieves triaxiality and enables the PC matrix in the SWZ to deform in shear. The amount of matrix shear deformation then depends on the magnitude of the shear stresses in the cavitated material as given by the imbalance between the principal stresses. Observation of the shear texture in the xy and yz planes of the SWZ but not the xz plane suggests that σ_2 and σ_3 are comparable and less than σ_1. The elastic stresses in the SWZ are not easily calculated. Alternatively, it is possible to calculate σ_1 and σ_2 in the CYZ from slip line theory and specifically to calculate the values at the boundary of the CYZ where the stresses in the plastic zone and the surrounding elastic material are the same. From slip line theory,[6] the principal stresses along the x-axis are given by

$$\sigma_y = \sigma_1 = \frac{2}{\sqrt{3}}\sigma_T[1 + \ln(r/a)] \quad (1)$$

$$\sigma_x = \sigma_2 = \frac{2}{\sqrt{3}}\sigma_T[\ln(r/a)], \quad (2)$$

and for the fully plane strain condition,

$$\sigma_z = \sigma_3 = 0.5(\sigma_1 + \sigma_2) = \frac{2}{\sqrt{3}}\sigma_T[0.5 + \ln(r/a)] \quad (3)$$

where σ_T is the tensile yield stress of the blend; a, the notch radius; and r, the distance from the tip of the CYZ to the notch origin.

It is apparent from eqs. (1)–(3) that the stresses in the CYZ increase away from the notch root in a manner that depends only on the distance from the notch root, not on the remote stress. Increasing the remote stress causes the zone to grow outward and the stresses at the tip of the CYZ to increase correspondingly. Cavitation begins when the mean stress $\sigma_m = (\sigma_1 + \sigma_2 + \sigma_3)/3$ at the tip of CYZ reaches the critical value $\sigma_{m,c}$. As the remote stress increases further, the CYZ continues to grow; however, cavi-

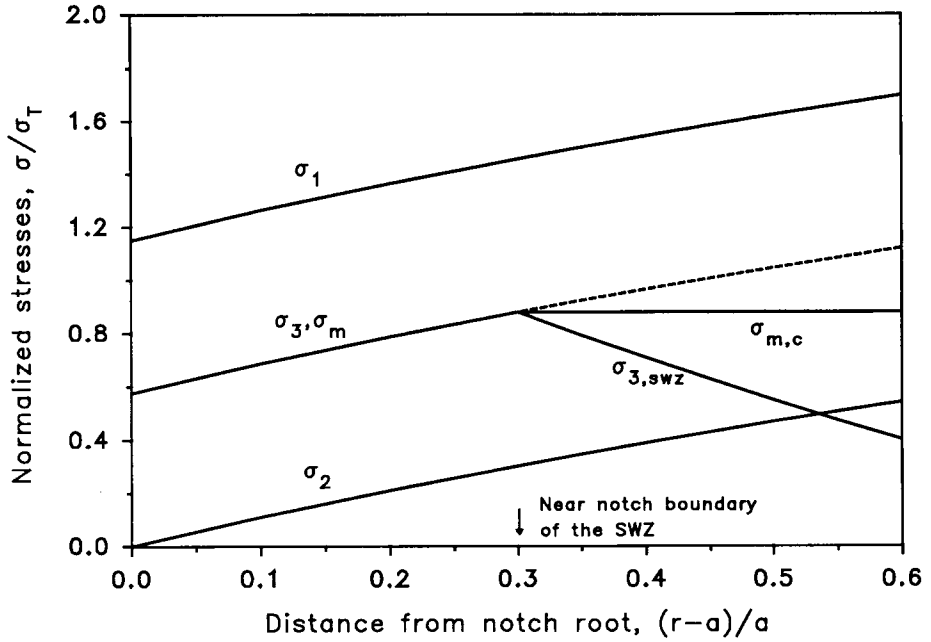

Figure 4 The stress distribution along the x-axis in the CYZ ahead of a semicircular notch.

tation now relieves the local stress when it exceeds the critical value. It is assumed that due to cavitation the mean stress in the SWZ is essentially constant and equal to the critical mean stress (Fig. 4). If it is further assumed that cavitation relieves specifically σ_3, while σ_1 and σ_2 are not strongly affected and are given by slip line theory, it is possible to estimate the decrease in σ_3 as the CYZ grows away from the notch root. The calculated stress distribution along the x-axis at a remote stress of 0.8 σ_T is given in

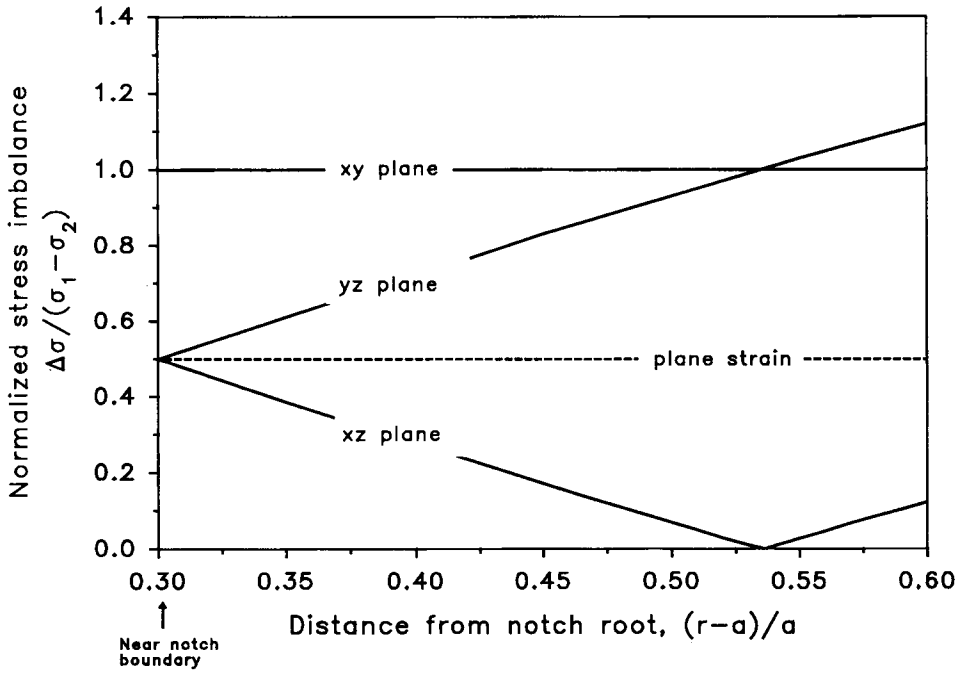

Figure 5 The stress imbalances in the near notch region of the SWZ.

Figure 4. When the distance from the notch root is less than $0.3a$, σ_m is less than the critical value for cavitation and σ_3 is calculated according to the plane strain condition. The critical value is achieved at the position $0.3a$, the near notch boundary of the SWZ. Between $0.3a$ and the tip of the CYZ at $0.6a$, σ_m is constant and equal to the critical value while σ_3 decreases as shown.

The corresponding normalized stress imbalances along the x-axis between $0.3a$ and $0.6a$ are plotted in Figure 5. In the fully plane strain condition, the stress imbalance is the same in the yz and xz planes as indicated by the dashed line and is about half that in the xy plane. This predicts that the shear texture should be strongest in the xy plane and comparable in the yz and xz planes. This was not observed. Since the triaxiality was relieved by cavitation, the actual stress state in the SWZ was not fully plane strain. The effect of decreasing σ_3 was to increase the stress imbalance in the yz plane until it approached or even exceeded the stress imbalance in the xy plane and to decrease the stress imbalance in the xz plane. The relative magnitudes calculated for these stress imbalances were consistent with the observation of a strong shear texture in both the xy and yz planes and essentially no shear texture in the xz plane. The calculations included only the near notch region of the SWZ. In the far notch region, both σ_2 and σ_3 were significantly smaller than was σ_1, and, qualitatively, the stress imbalances would resemble those calculated for the near notch region.

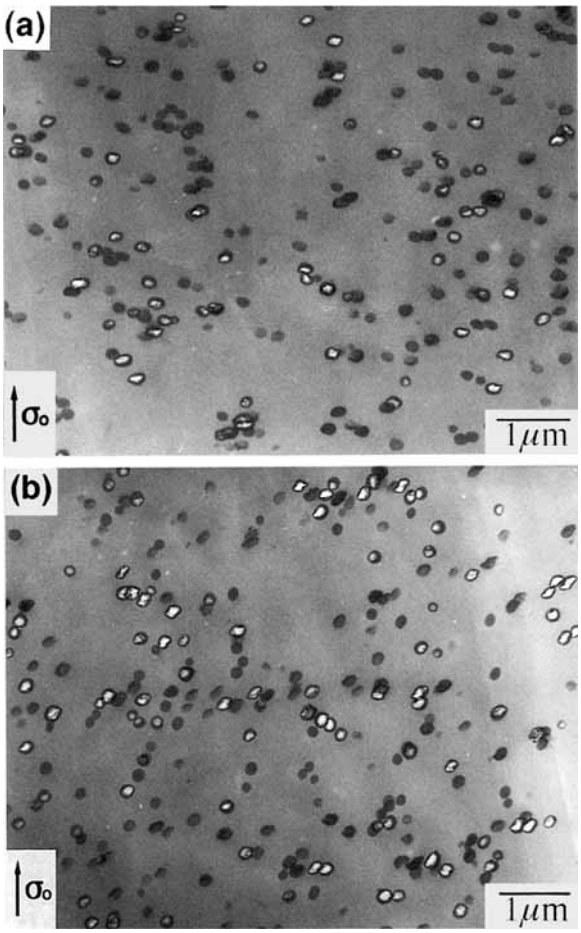

Figure 6 Transmission electron micrographs of sections from the SWZ in PC with 2% PL at 0.8 σ_T: (a) the near notch region; (b) the far notch region.

Nanoscale Deformation of Blend with 2% PL

Micrographs of the undeformed blend with 2% PL showed uniform, well-dispersed spherical particles about 0.2 μm in diameter. After the blend was loaded to 0.8 σ_T, sections were obtained at various locations in the CYZ and the SWZ. None of the rubber particles in the region of the CYZ between the notch root and SWZ were cavitated. Furthermore, the particles in this region retained their circular shape, which indicated that the local shear strain in the matrix was not large enough to cause distortion of the particles.

A typical micrograph from the near notch region of the SWZ in Figure 6(a) shows some cavitated rubber particles. In general, cavitated particles in the 2% PL blend were randomly distributed, although, occasionally, two particles close together would both be cavitated. The far notch region of the SWZ was similar to the near notch region with randomly distributed cavitated particles [Fig. 6(b)]. The primary difference was a higher percentage of cavitated particles in the far notch region. There was no apparent directionality to the cavitation in either the near notch region or the far notch region that correlated with the loading direction.

The volume parameters, specifically particle size and volume fraction of cavitated particles, were reconstructed from features measured in the micrographs of thin sections using well-established methods for randomly distributed spherical particles of uniform size.[7] The average diameter of either particles or voids D_V was calculated from the average area diameter D_A according to

$$\frac{D_A}{D_V} = \frac{\left[1 + \frac{\pi D_V}{4t}\right]}{\left[1 + \frac{D_V}{t}\right]} \tag{4}$$

Table I Number Fraction of Cavitated Particles in the SWZ

	Near Notch Region			Far Notch Region		
	Fraction of Cavitated Particles			Fraction of Cavitated Particles		
Rubber Content	Area $N_{A,C}/N_{A,R}$	Volume $N_{V,C}/N_{V,R}$	Cavity Diameter $D_{V,C}$ (μm)	Area $N_{A,C}/N_{A,R}$	Volume $N_{V,C}/N_{V,R}$	Cavity Diameter $D_{V,C}$ (μm)
2% PL	0.20	0.30	0.11	0.53	0.78	0.11
5% PL	0.15	0.22	0.11	0.35	0.49	0.12
10% PL	0.15	0.22	0.11	0.35	0.47	0.15

where t, the thickness of the section used to obtain D_A, was typically between 90 and 120 nm. When the magnitudes of t and D_V are comparable, the number of particles or voids per unit volume can be calculated from[8]

$$N_V = \frac{N_A}{t + D_V} \tag{5}$$

The number fraction of cavitated particles can then be calculated from

$$\frac{N_{VC}}{N_{VR}} = \left[\frac{N_{AC}}{N_{AR}}\right]\left[\frac{D_{VR} + t}{D_{VC} + t}\right] \tag{6}$$

where $N_{V,R}$ and $N_{V,C}$ are the total number of rubber particles and the number of cavitated particles per unit volume, respectively, and $N_{A,R}$ and $N_{A,C}$ are the total number of rubber particles and the number of cavitated particles per unit area measured from the micrographs. The results are summarized in Table I. The uncavitated particle size was 0.18 μm, slightly less than the 0.20 μm determined by SEM.[9] Cavitation produced a void typically 0.10 μm in diameter and an increase in the particle size to 0.21 μm. The fraction of cavitated particles in the 2% PL blend increased from 0.30 in the near notch region of the SWZ to 0.78 in the far notch region.

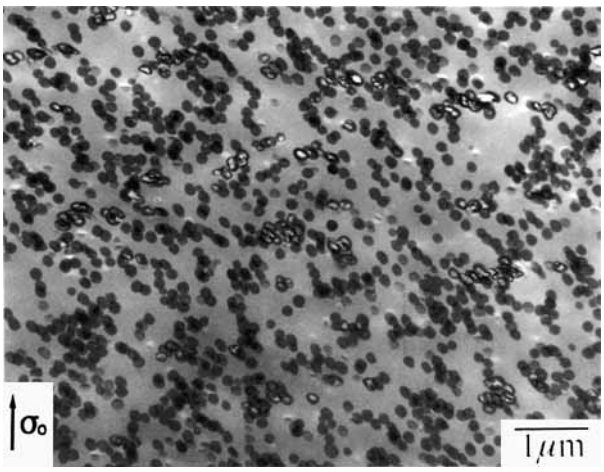

Figure 7 Transmission electron micrograph of a section from the near notch region of the SWZ in PC with 10% PL at 0.8 σ_T.

Nanoscale Deformation of Blend with 10% PL

The rubber in the 10% PL blend was dispersed as isolated particles together with clumps or strings of particles. Again, the blend was loaded to 0.8 σ_T and sections were obtained at various locations in the CYZ and the SWZ. As with the 2% PL blend, the micrographs from the region of the CYZ between the notch root and SWZ did not reveal any cavitated or deformed rubber particles. The near notch region of the SWZ contained single cavitated particles (Fig. 7). The single cavitated particles could either be isolated or could be in a clump with uncavitated particles. The micrograph also showed clumps where most of the particles were cavitated. The speckled texture seen in the optical microscope, which was especially distinctive in the xz plane where there were no shear lines, may have been caused by these clumps of cavitated particles.

Deformation of the 10% PL blend at the nanoscale changed from isotropic and random in the near notch region to anisotropic and cooperative in the far notch region. A low magnification micrograph of a section from the far notch region of the SWZ shows numerous parallel dark, wavy lines that are oriented approximately perpendicular to the loading direction (Fig. 8). They corresponded closely in orientation and size to the irregular wavy lines that characterized the microscale texture in optical micrographs of the far notch region.

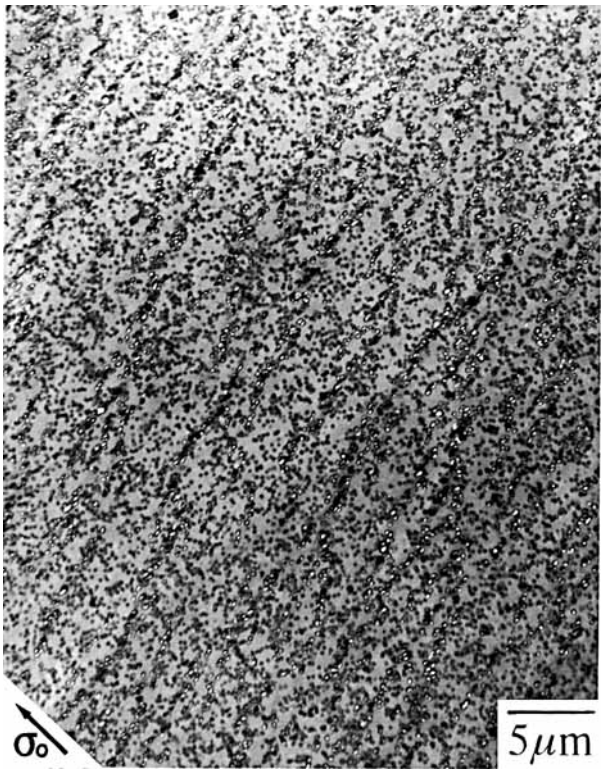

Figure 8 Low magnification electron micrograph of a section from the far notch region of the SWZ in PC with 10% PL at 0.8 σ_T.

At higher magnification, the wavy dark lines were seen to consist of rows of cavitated particles [Fig. 9(a)]. The cavitated arrays were thin with a broad range in length; they typically incorporated 1–4 cavitated particles in the thickness direction and 8–35 cavitated particles in the length. Sometimes, the cavitated particles in the array were also distorted, which suggested that, locally, the matrix was highly deformed. Most of the particles outside the arrays were not cavitated, nor were they distorted. This emphasized the nanoscale inhomogeneity of deformation in the far notch region of the SWZ. The SWZ in the blend with 5% PL also contained arrays of cavitated rubber particles, although the arrays were shorter and thinner than in the 10% PL blend and were further apart. The fraction of particles that cavitated was about the same in the 5 and 10% PL blends and increased from 0.22 in the near notch region to almost 0.50 in the region of the cavitated arrays.

The three-dimensional shape of the cavitated arrays was obtained by comparing sections from the three orthogonal planes. In the *yz* section [Fig. 9(b)], rows of cavitated particles oriented normal to the loading direction formed arrays that were similar in size and shape to the arrays seen in the *xy* plane. The cavitated particles also were not randomly distributed in the *xz* plane, but in this plane, the cavitated particles were concentrated in regions that

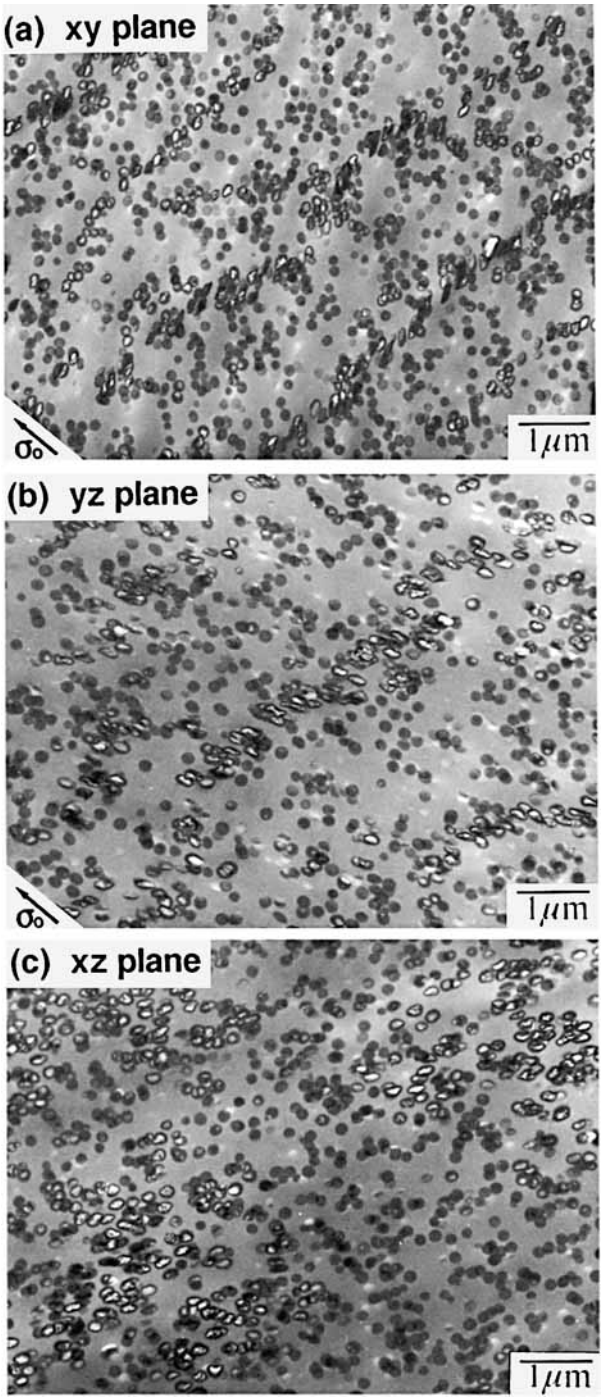

Figure 9 Transmission electron micrographs of sections from the far notch region of the SWZ in PC with 10% PL at 0.8 σ_T: (a) *xy* plane; (b) *yz* plane; (c) *xz* plane.

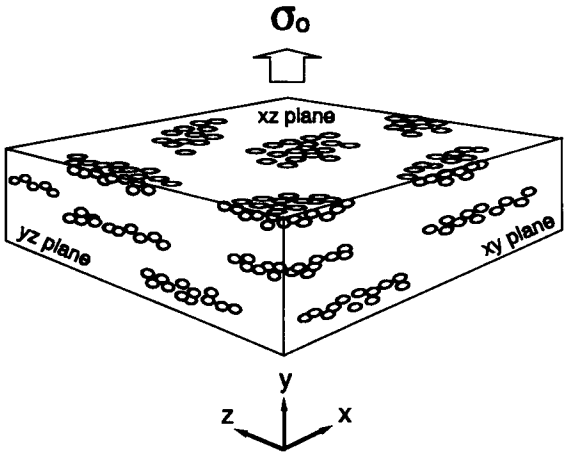

Figure 10 Three-dimensional representation of cavitated arrays in the far notch region of the SWZ in PC with 10% PL at 0.8 σ_T. Uncavitated particles are not shown in the drawing.

were more or less circular with no clear directionality [Fig. 9(c)].

The three views of the cavitated arrays were combined to produce the three-dimensional sketch in Figure 10 of disk-shaped, cavitated domains. The disks were largest in the 10% PL blend, smaller but still present in the 5% PL blend, and not observed in the 2% PL blend. This suggested that as the average particle separation decreased from 2% PL to 10% PL there was a change from virtually random cavitation to predominantly cooperative cavitation in the far notch region of the SWZ.

Although the cavitated arrays showed certain crazelike features, they did not initiate catastrophic fracture. Figure 11 shows a micrograph from the far notch region of the SWZ after the load on the 10% PL blend was increased to 0.9 σ_T. Cavitated arrays were no longer clearly defined; instead, the entire area of the micrograph contained cavitated and uncavitated particles that were highly elongated in the loading direction. The drawn matrix ligaments between cavitated particles of the arrays did not fracture; instead, regions separating the arrays deformed by particle cavitation and matrix extension. As a result, definition of the arrays was lost and the entire section contained cavitated and uncavitated particles that were highly elongated in the loading direction. Using the particles as deformation markers, the material appeared to be uniformly extended an amount close to the natural draw of the PC matrix, about 100%. A similar cellular morphology is observed when irregularly shaped crazes in styrene/rubber block copolymers broaden in the stress direction.[10-12] The irregular shape, the indistinct boundaries, and the strong fibrils or ligaments of the craze or cavitated array are the common features.

Cavitated arrays in the 10% PL blend were also observed at lower temperatures. Arrays in the far notch region of the SWZ of the blend loaded to 0.8 σ_T at −40°C had essentially the same morphological features as those of arrays that formed during loading at ambient temperature (Fig. 12). The cavitated arrays can impart higher impact strength, especially at low temperatures, if energy is absorbed more efficiently by cooperative cavitation than by random cavitation. However, because a low loading rate was used to produce the cavitated arrays in Figure 12,

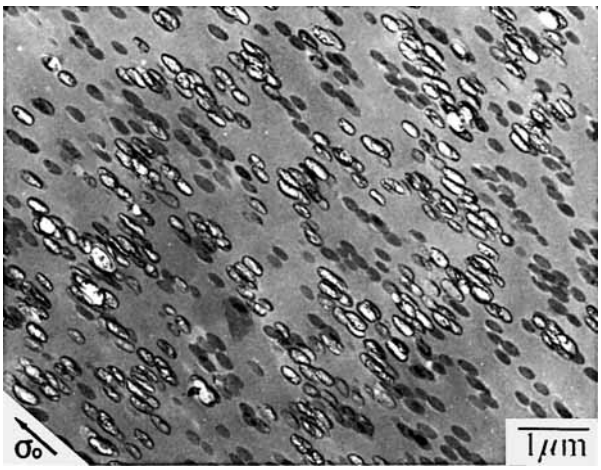

Figure 11 Transmission electron micrograph of a section from the far notch region of the SWZ in PC with 10% PL at 0.9 σ_T.

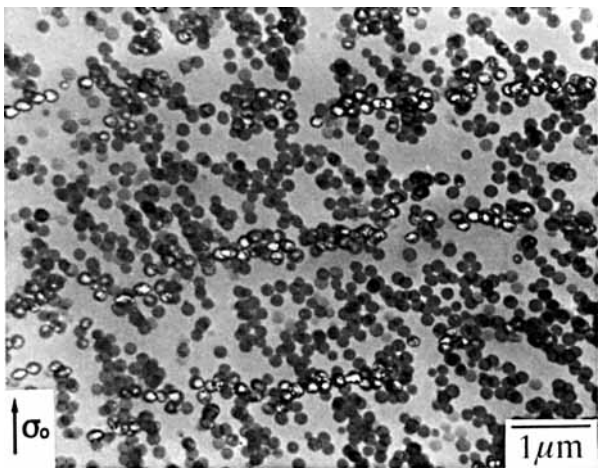

Figure 12 Transmission electron micrograph of a section from the far notch region of the SWZ in PC with 10% PL loaded to 0.8 σ_T at −40°C.

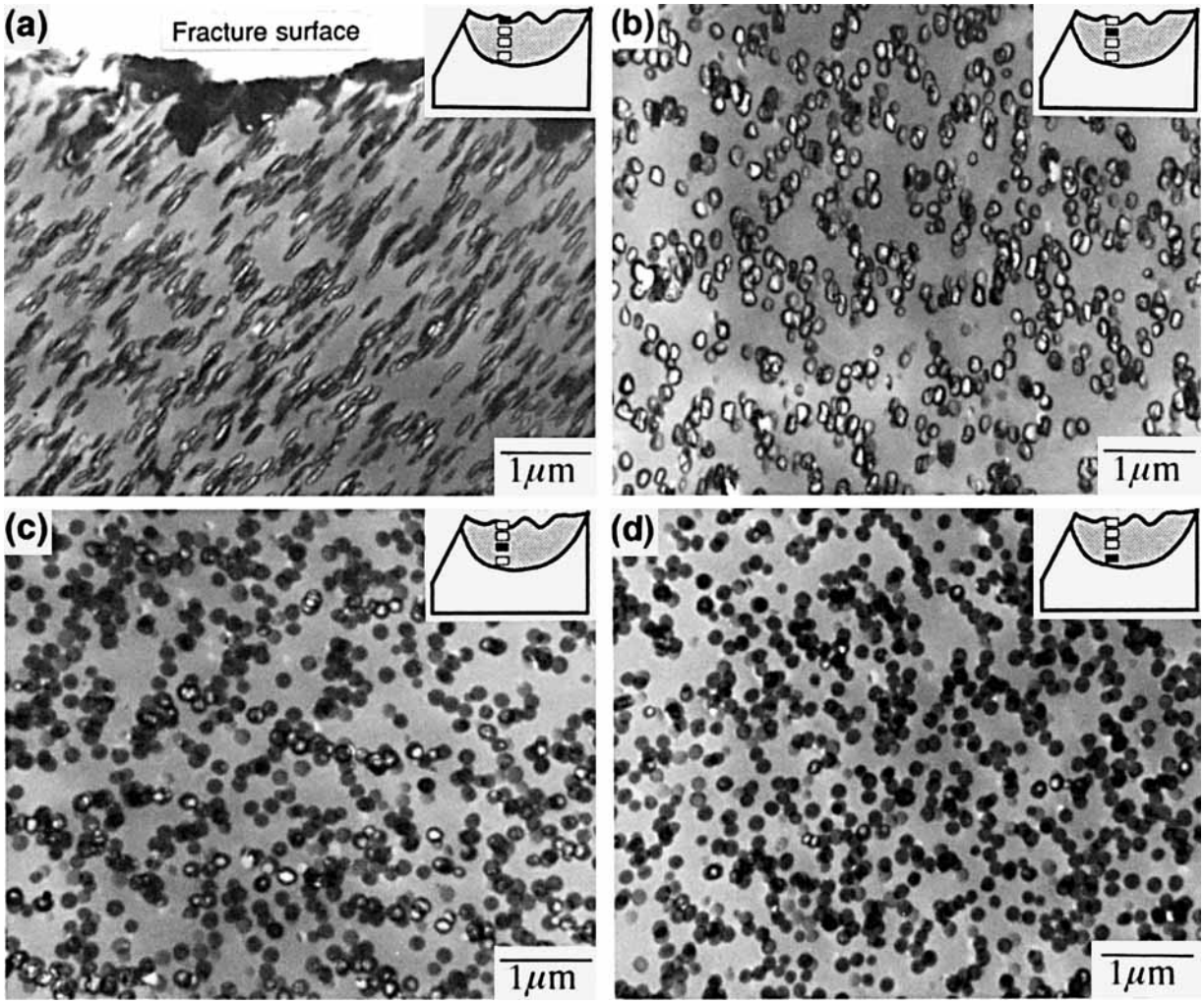

Figure 13 Transmission electron micrographs of sections from the SWZ in PC with 10% PL impacted at −20°C: (a) close to the fracture surface; (b) 140 μm from the fracture surface; (c) 350 μm from the fracture surface; (d) 500 μm from the fracture surface. The crack propagated from left to right.

the results may not translate directly to impact experiments carried out at high speeds.

PC with 10% PL is ductile at −20°C with an Izod impact strength of 555 J/m. A specimen that had been impacted at −20°C was sectioned through the SWZ that adjoined the fracture site, and the four micrographs in Figure 13 show the rubber particles at various distances from the fracture surface. Close to the fracture surface, the particles were virtually all cavitated and they were elongated about 100% at an angle to the fracture plane [Fig. 13(a)]. This is typical of the deformation at a shear tearing fracture.[3] Slightly further from the fracture surface, the particles were all cavitated but they were not elongated [Fig. 13(b)]. In between this position, and the position furthest from the fracture surface where a few cavitated particles were randomly distributed [Fig. 13(d)], linear arrays of cavitated particles were observed [Fig. 13(c)]. The arrays were indistinguishable from those that formed at low loading rates in the far notch region of the SWZ.

If the particle morphology at the various positions in the SWZ is taken as representing a sequence of events, the cavitated arrays appear to be transitional from random cavitation of isolated particles to complete cavitation of all the particles. Irreversible deformation is seen as beginning with random cavitation of the rubber particles in response to a mean stress condition. If the interparticle spacing is small enough, cavitation of a single particle leads to co-

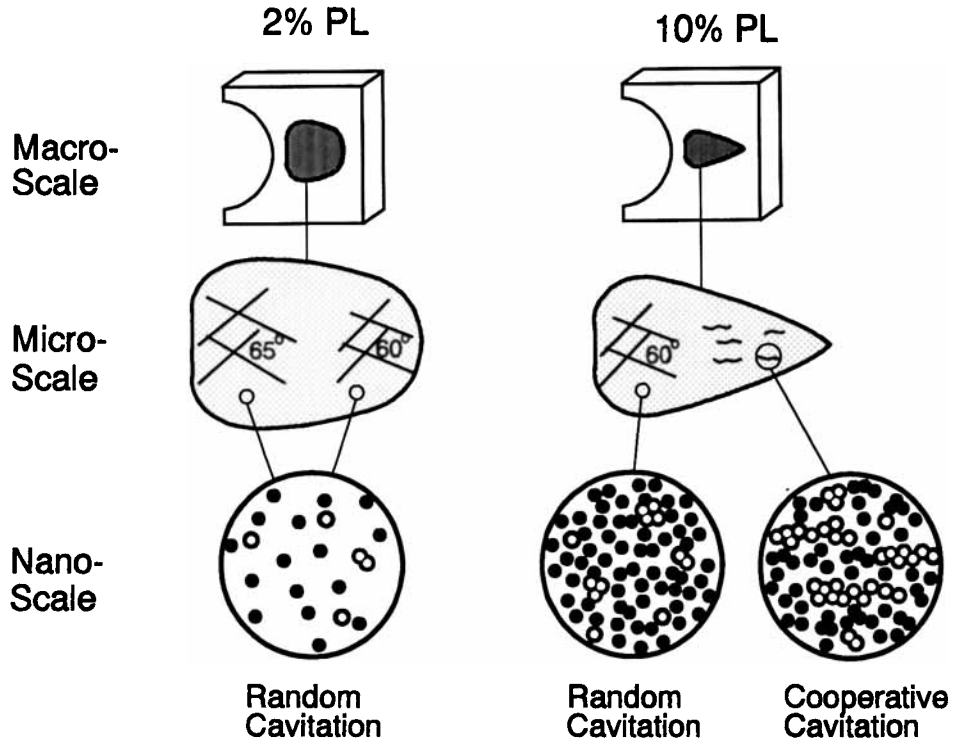

Figure 14 Hierarchical models of the deformation zone ahead of a semicircular notch in blends of PC with PL rubber.

operative cavitation of neighboring particles. The mechanism of particle–particle interaction that results in cavitated arrays may be controlled by the major principal stress after the triaxiality is largely relieved by random cavitation. The PC ligaments between cavitated particles in the array do not fracture; instead, the arrays lose their definition when particles that are not in arrays cavitate. Subsequently, all the cavitated particles are drawn out during ductile yielding of the matrix.

The transitional role of cavitated arrays may be one reason why they have not been more frequently described, especially in studies that utilize high-speed testing. Arrays are not readily observed by postfracture analysis of impacted specimens; to find them, examination of a specific region of the damage zone, located some distance from the fracture surface, is required. The sequence of deformation events inferred from analysis of impacted specimens is qualitatively the same as that observed at low loading rates, and, in addition, low-rate experiments have the advantage that deformation can be halted and transitional stages examined. A relatively minor difference, that fewer particles cavitate in the low-rate experiment, may reflect the different rate sensitivities of particle cavitation and matrix shearing or the different stress states at an Izod notch and a semicircular notch.

Concluding Remarks on the Hierarchy of Deformation

The deformation mechanisms at the macro-, micro-, and nanoscales are schematically summarized in Figure 14. At the macroscale, the deformation zone that forms in the triaxial stress field ahead of a semicircular notch consists of a core yielding zone (CYZ) that grows out of the notch root, together with a stress-whitened zone (SWZ) that appears some distance ahead of the notch root. The condition for particle cavitation, as determined from the position of the near notch boundary of the SWZ, is independent of the rubber content. This is consistent with the nanoscale observation that particle cavitation in the near notch region of the SWZ occurs randomly without particle–particle interaction effects.

At the microscale, the texture of the near notch region of the SWZ consists of fine shear lines that intersect at an angle of about 60°. It is thought that cavitation of the rubber particles relieves triaxiality and enables the PC matrix in the SWZ to deform

in shear. The appearance of the shear texture in the *xy* and *yz* planes (parallel to the loading direction) but not the *xz* plane (normal to loading) is consistent with the relative magnitudes of the redistributed shear stresses in the three orthogonal planes.

The microscale shear texture observed in the optical microscope has no corresponding nanoscale features in transmission electron micrographs of thin sections. At the nanoscale, rubber particles or clumps of rubber particles are randomly cavitated in those regions of the SWZ that exhibit the shear texture. With increasing rubber content, the far notch region of the SWZ takes on a narrower, more elongated shape and the microscale texture changes from intersecting shear lines to parallel wavy lines. These coarse, wavy lines seen in the optical microscope correspond at the nanoscale to long arrays of cooperatively cavitated and deformed rubber particles. In another study of particle cavitation in PC blends with similar core–shell particles, the particle concentration, 3.3%, was too low for the arrays to be observed.[13] The interparticle distance requirements for cooperative cavitation are usually discussed with reference to interacting local elastic stress fields.[14] Although elastic arguments may apply to cooperative cavitation of particles in brittle matrices,[15] with a ductile thermoplastic matrix in an unbalanced triaxial stress state, it is appropriate to consider the contribution of localized shear yielding.

The cavitated arrays in PC blends, oriented normal to the loading direction, resemble the craze arrays observed in microlayers with many alternating layers of styrene–acrylonitrile copolymer (SAN) and PC.[16,17] Here, a cavitational mechanism, crazing of the SAN layer, produces a local stress concentration at the interface with PC. With good adhesion between SAN and PC, a small plastic zone forms in the PC layer at the craze tip. Cooperative crazing from one SAN layer to the next is attributed to impingement of the craze tip plastic zone in the thin PC layer on the next SAN layer. The result is a row of SAN crazes separated by PC ligaments. The possibility that arrays of cavitated rubber particles in PC form by a similar mechanism should be considered.

Cooperative cavitation of rubber particles to form voided arrays is followed by pullout of the matrix ligaments between particles and distortion of the voided particles. The matrix ligaments are strong enough that they do not fracture, and, thereby, formation of a critical-size crack that would lead to catastrophic fracture is prevented. Higher strains are accommodated by deformation of the material between arrays until the matrix, together with both cavitated and uncavitated particles, is uniformly extended. The possibility that cavitation can occur cooperatively has implications for the impact strength of blends with higher concentrations of rubber particles. The possibility that particle–particle interactions facilitate cavitation and promote matrix shear deformation is especially relevant to low-temperature impact strength.

This research was generously supported by EniChem America Inc. and the National Science Foundation, I/UCRC Program, Grant EEC-9320055.

REFERENCES

1. M. Ishikawa, I. Narisawa, and H. Ogawa, *J. Polym. Sci. Polym. Phys. Ed.*, **15,** 1791 (1977).
2. C. Cheng, A. Hiltner, E. Baer, P. R. Soskey, and S. G. Mylonakis, *J. Appl. Polym. Sci.*, **52,** 177 (1994).
3. C. Cheng, N. Peduto, A. Hiltner, E. Baer, P. R. Soskey, and S. G. Mylonakis, *J. Appl. Polym. Sci.*, **53,** 513 (1994).
4. A. Lazzeri and C. B. Bucknall, *J. Mater. Sci.*, **28,** 6799 (1993).
5. M. Ma, K. Vijayan, A. Hiltner, and E. Baer, *J. Mater. Sci.*, **24,** 2687 (1989).
6. R. Hill, *The Mathematical Theory of Plasticity,* Clarendon, Oxford, 1950.
7. P. L. Goldsmith, *Br. J. Appl. Phys.*, **18,** 813 (1967).
8. M. A. Williams, in *Practical Methods in Electron Microscopy,* A. M. Glauert, Ed., North-Holland, Amsterdam, 1977, Vol. 6.
9. C. V. Berney, R. E. Cohen, and F. S. Bates, *Polymer,* **23,** 1222 (1982).
10. C. E. Schwier, A. S. Argon, and R. E. Cohen, *Philos. Mag.*, **A52,** 581 (1985).
11. A. S. Argon, R. E. Cohen, O. S. Gebizlioglu, and C. E. Schwier, in *Advances in Polymer Science 52/53,* H. H. Kausch, Ed., Springer-Verlag, New York, 1983.
12. B. Koltisko, A. Hiltner, and E. Baer, *J. Polym. Sci. Polym. Phys. Ed.*, **24,** 2167 (1986).
13. D. S. Parker, H.-J. Sue, J. Huang, and A. F. Yee, *Polymer,* **31,** 2267 (1990).
14. S. Wu, *Polymer,* **26,** 1855 (1985).
15. H.-J. Sue, E. I. Garcia-Meitin, and N. A. Orchard, *J. Polym. Sci. Part B Polym. Phys.*, **31,** 595 (1993).
16. D. Haderski, K. Sung, J. Im, A. Hiltner, and E. Baer, *J. Appl. Polym. Sci.*, **52,** 121 (1994).
17. K. Sung, D. Haderski, A. Hiltner, and E. Baer, *J. Appl. Polym. Sci.*, **52,** 147 (1994).

Received September 2, 1994
Accepted October 3, 1994